

Complex decay chains of top and bottom squarks

Jonathan Eckel^{1*}, Shufang Su^{1†}, Huanian Zhang^{1‡}

¹ *Department of Physics, University of Arizona, Tucson, Arizona 85721*

Abstract

Current searches for the top squark mostly focus on the decay channels of $\tilde{t}_1 \rightarrow t\chi_1^0$ or $\tilde{t}_1 \rightarrow b\chi_1^\pm \rightarrow bW\chi_1^0$, leading to $tt/bbWW + \cancel{E}_T$ final states for top squark pair production at the LHC. In supersymmetric scenarios with light gauginos other than the neutralino lightest supersymmetric particle (LSP), different decay modes of the top squark could be dominant, which significantly weaken the current top squark search limits at the LHC. Additionally, new decay modes offer alternative discovery channels for top squark searches. In this paper, we study the top squark and bottom squark decay in the Bino-like LSP case with light Wino or Higgsino next-to-LSPs (NLSPs), and identify cases in which additional decay modes become dominant. We also perform a collider analysis for top squark pair production with mixed top squark decay final states of $\tilde{t}_1 \rightarrow t\chi_2^0 \rightarrow th\chi_1^0$, $\tilde{t}_1 \rightarrow b\chi_1^\pm \rightarrow bW\chi_1^0$, leading to the $bbbbjj\ell + \cancel{E}_T$ collider signature. The branching fraction for such decay varies between 25% and 50% for a top squark mass larger than 500 GeV with $M_2 = M_1 + 150$ GeV. At the 14 TeV LHC with 300 fb^{-1} integrated luminosity, the top squark can be excluded up to about 1040 GeV at the 95% C.L., or be discovered up to 940 GeV at 5σ significance.

* eckel@physics.arizona.edu

† shufang@email.arizona.edu

‡ fantasyzhn@email.arizona.edu

I. INTRODUCTION

The discovery of a 125 GeV Higgs at the Large Hadron Collider (LHC) [1, 2] motivates the consideration of new physics beyond the Standard Model (SM). In the SM, the Higgs receives unstable quadratically divergent radiative corrections to its mass from the top quark loop. An unnatural cancellation is needed to recover the light physical Higgs mass, which is the so called “Hierarchy problem” [3]. Supersymmetry (SUSY) provides a solution to the naturalness problem by introducing superpartners to the SM particles, with interactions following the SUSY relations. The quadratic divergence from the superpartners cancels that of the SM particles, with the remnant contributions being only logarithmically divergent. Given the large top Yukawa coupling, the top and top squark (referred to as stop) sectors of the Minimal Supersymmetric Standard Model (MSSM) provide the largest radiative corrections to the Higgs mass. Stop masses can not be too heavy in order to avoid excessive fine tuning of the Higgs mass. A TeV scale stop typically leads to fine tuning of about 1% [4]. Given the tight connection between the stop and Higgs sectors, it is important to fully explore the discovery potential of the stop at the LHC.

Most of the current searches for the light stop focus on the decay $\tilde{t}_1 \rightarrow t\chi_1^0$ or $\tilde{t}_1 \rightarrow b\chi_1^\pm \rightarrow bW\chi_1^0$, with χ_1^0 being the stable lightest supersymmetric particle (LSP) appearing as missing energy (\cancel{E}_T) at colliders. For stop pair production at the LHC, such processes lead to $t\bar{t} + \cancel{E}_T$ or $b\bar{b}WW + \cancel{E}_T$ final states. However, due to the large SM backgrounds from $t\bar{t}$, searches for the stop can be very challenging. The current limits from ATLAS and CMS experiments exclude stops with masses up to about 645 GeV for a light neutralino LSP [5–10]. For small mass spitting between the stop and the LSP, $\tilde{t}_1 \rightarrow c\chi_1^0$ and $\tilde{t}_1 \rightarrow bff'\chi_1^0$ has been studied [11, 12], with limits for stop masses around 240 to 270 GeV. Searches for the second stop with $\tilde{t}_2 \rightarrow \tilde{t}_1 Z/h$ have also been performed, which provide stop mass limits around 540 to 600 GeV [13–15]. Stop decay with a gravitino LSP has also been studied in Ref. [13, 16].

Similarly, the current bottom squark (referred to as sbottom) searches mostly focus on $\tilde{b}_1 \rightarrow b\chi_1^0$, with $b\bar{b} + \cancel{E}_T$ being the dominant search channel. Given data collected at the LHC 7/8 TeV, sbottoms with masses up to 700 GeV are excluded [11, 17, 18]. Searches based on sbottom decay of $\tilde{b}_1 \rightarrow b\chi_2^0 \rightarrow bZ/h\chi_1^0$ exclude sbottom masses between 340 and 600 GeV [19, 20]. $\tilde{b}_1 \rightarrow t\chi_1^\pm \rightarrow tW\chi_1^0$ decay has also been studied in multi-lepton final

states [20–23], which excludes sbottom masses around 440 –590 GeV. The left-handed sbottom mass is related to the left-handed stop mass since they are controlled by the same soft SUSY breaking mass parameter. In this paper, we also study the left-handed sbottom decay patterns, as well as its collider signatures.

There are other theoretical studies in the literature on the stop searches at the LHC, mostly focusing on the light stop decaying to light generation quarks [24–28] with little missing energy, which mimics the WW signal at the LHC [29–33] or multi- b jets final states from a light stop [34]. For the sbottom, in a parameter space with highly degenerate sbottom and LSP masses, a strategy has been proposed to search for sbottom based on boosting bottoms through an energetic initial radiation jet [35].

The current stop and sbottom search limits, however, could be significantly weakened when other decay modes open, which could occur in many regions of MSSM parameter space. On the other hand, the opening of new channels offers alternative discovery potential for stops and sbottoms at the LHC. It is thus important to analyze all possible stop and sbottom decay patterns to fully explore the discovery potential at the 14 TeV LHC.

Even under the usual assumption of a Bino-like LSP, the existence of other light neutralino states, for example, Wino-like or Higgsino-like next-to-LSPs (NLSPs) could lead to new decay channels for the stop. For instance, \tilde{t}_1 could decay to $t\chi_{2,3}^0$, with $\chi_{2,3}^0$ further decaying to $Z\chi_1^0, h\chi_1^0$. Given the relatively large $SU(2)_L$ coupling and top Yukawa coupling, compared to the $U(1)_Y$ coupling relevant for the Bino-like LSP, decays to $t\chi_{2,3}^0$ could even be dominant despite the phase space suppression. In this paper, we study the stop and sbottom decay branching fractions for the Wino- or Higgsino-like NLSP case, considering the minimal mixing and the maximal mixing scenarios in the stop sector, and outline the main search channels for the stops and bottoms at the LHC.

Given the discovery of the SM-like Higgs boson at the LHC, we can now use final states with a Higgs boson to search for new physics beyond the SM. To demonstrate the 14 TeV LHC reach with those complex stop decay channels, we performed a sample collider analysis with a Higgs in the final state: $pp \rightarrow \tilde{t}_1\tilde{t}_1^*$ with mixed stop decay final states of $\tilde{t}_1 \rightarrow t\chi_2^0 \rightarrow th\chi_1^0$, $\tilde{t}_1 \rightarrow b\chi_1^\pm \rightarrow bW\chi_1^0$, leading to the $bbbbjj\ell + \cancel{E}_T$ collider signature with the assumption of the branching fraction of $h \rightarrow b\bar{b}$ being the SM value of 57.7%. The branching fraction for such decay could vary between 25% and 50% for a stop mass larger than 500 GeV with $M_2 = M_1 + 150$ GeV. By designing selection cuts to identify

the signal while suppressing SM backgrounds, we obtained the 95% C.L. exclusion limit as well as the 5σ discovery reach in $m_{\tilde{t}_1}$ versus $m_{\chi_1^0}$ plane at the 14 TeV LHC with 300 fb^{-1} integrated luminosity. Note that other Higgs decay channels: $h \rightarrow WW, ZZ, \gamma\gamma, \tau\tau$ are not considered in our current analyses, which could lead to interesting multi-lepton final states or extremely clean (although suppressed) $\gamma\gamma$ signatures. Final states with $\chi_2^0 \rightarrow Z\chi_1^0$ are left for future studies.

The rest of the paper is organized as the following. In Sec. II, we present the third generation squark sector in the MSSM and discuss its connection to the Higgs sector. In Sec. III, we discuss the stop and sbottom decays for various scenarios, as well as the collider signatures for stop/sbottom pair production. In Sec. IV, we summarize the current and future LHC stop and sbottom search results from both ATLAS and CMS. In Sec. V, we investigate the 14 TeV reach of the stop via final states with a Higgs. In Sec. VI, we conclude.

II. MSSM STOP SECTOR

In this study, we work in the MSSM and focus primarily on the third generation squark sector. We decouple other SUSY particles: the gluino, sleptons, and the first and second generation squarks. We also decouple the non-SM Higgs particles by setting M_A large. The remaining SUSY particles in the model are the third generation squarks, the neutralinos and charginos.

The gauge eigenstates for the superpartners of the top and bottom quarks are $(\tilde{t}_L, \tilde{b}_L), \tilde{t}_R$ and \tilde{b}_R , with the left-handed states grouped as an $\text{SU}(2)_L$ doublet and the right-handed states as singlets. The mass matrix for the stop sector is

$$\mathbf{m}_{\tilde{t}}^2 = \begin{pmatrix} M_{3SQ}^2 + m_t^2 + \Delta_{\tilde{u}_L} & m_t \tilde{A}_t \\ m_t \tilde{A}_t & M_{3SU}^2 + m_t^2 + \Delta_{\tilde{u}_R} \end{pmatrix}, \quad (1)$$

with M_{3SQ}^2 and M_{3SU}^2 representing the soft SUSY breaking masses for \tilde{t}_L and \tilde{t}_R , m_t^2 term coming from the F-term contribution in the SUSY Lagrangian and the Δ terms coming from the D-term contribution. The off-diagonal term \tilde{A}_t is given by:

$$\tilde{A}_t = A_t - \mu / \tan \beta, \quad (2)$$

for A_t representing the trilinear coupling and μ representing the supersymmetric bilinear mass term in the Higgs sector. $\tan\beta = \langle H_u^0 \rangle / \langle H_d^0 \rangle$ is the ratio of the vacuum expectation values of H_u^0 and H_d^0 in the MSSM.

The stop mass matrix can be diagonalized with a stop mixing angle θ_t :

$$\begin{pmatrix} \tilde{t}_1 \\ \tilde{t}_2 \end{pmatrix} = \begin{pmatrix} \cos\theta_t & -\sin\theta_t \\ \sin\theta_t & \cos\theta_t \end{pmatrix} \begin{pmatrix} \tilde{t}_L \\ \tilde{t}_R \end{pmatrix}, \quad (3)$$

with mass eigenstates \tilde{t}_1, \tilde{t}_2 : $m_{\tilde{t}_1} < m_{\tilde{t}_2}$. For $M_{3SQ} < (>) M_{3SU}$, \tilde{t}_1 is mostly left-handed (right-handed), while for $M_{3SQ}^2 \sim M_{3SU}^2$, $\tilde{t}_{1,2}$ could be a mixture of the left- and right-handed states.

Given the large top Yukawa coupling, the stop sector provides the dominant contribution to the radiative corrections of the SM-like Higgs mass in the MSSM. For $M_{3SQ} = M_{3SU} = M_{SUSY}$, the correction to the SM-like Higgs mass squared is [36]:

$$\delta m_h^2 = \frac{3}{4\pi^2} y_t^2 m_t^2 \sin^2\beta \left(\log \frac{M_{SUSY}^2}{m_t^2} + \frac{\tilde{A}_t^2}{M_{SUSY}^2} \left(1 - \frac{\tilde{A}_t^2}{12M_{SUSY}^2} \right) \right). \quad (4)$$

In the minimal mixing case with $\tilde{A}_t = 0$, a large M_{SUSY} around 5–10 TeV is needed to provide a SM-like Higgs mass of 125 GeV. In the maximal mixing case with $\tilde{A}_t = \sqrt{6}M_{SUSY}$, a relatively small $M_{SUSY} \sim \text{TeV}$ can be accommodated given the additional contribution from the \tilde{A}_t term. In the general MSSM when $M_{3SQ}^2 \neq M_{3SU}^2$, to provide a SM-like Higgs mass of 125 GeV, the light stop \tilde{t}_1 can still be as light as 200 GeV. A large mass splitting between the stop mass eigenstates (and a large \tilde{A}_t term), however, is typically needed, resulting in $m_{\tilde{t}_2} \gtrsim 500 \text{ GeV}$ in general [37, 38].

Similarly, the mass matrix for the sbottom is given as:

$$\mathbf{m}_{\tilde{b}}^2 = \begin{pmatrix} M_{3SQ}^2 + m_b^2 + \Delta_{\tilde{d}_L} & m_b \tilde{A}_b \\ m_b \tilde{A}_b & M_{3SD}^2 + m_b^2 + \Delta_{\tilde{d}_R} \end{pmatrix}, \quad (5)$$

with

$$\tilde{A}_b = A_b - \mu \tan\beta. \quad (6)$$

Given the suppression of the off-diagonal terms by the small bottom mass, mixing among the sbottom mass eigenstates is typically small. For $\tilde{A}_b \sim \text{TeV}$, the sbottom mixing angle is about one degree for $M_{3SQ} \sim M_{3SD} \sim \text{TeV}$.

Since the stop sector provides the dominant contribution to the Higgs mass corrections, we decouple the right-handed sbottom in our analysis. The left-handed sbottom mass, however, is determined by M_{3SQ} and could be relatively light. Given $m_b \tilde{A}_b, M_{3SQ}^2 \ll M_{3SD}^2$, the light sbottom mass eigenstate is mostly left-handed: $\tilde{b}_1 \sim \tilde{b}_L$. Although the sbottom corrections to the Higgs mass are small compared to the stop corrections, there can be significant modifications to the Higgs couplings, especially the bottom Yukawa coupling [39].

III. STOP DECAY

We consider the neutralino/chargino spectrum with a Bino-like LSP. For simplicity, we consider three representative scenarios:

- Case I, Bino-like LSP with decoupled Winos and Higgsinos: $M_1 < m_{\tilde{t}, \tilde{b}_1} \ll |\mu|, M_2$.
- Case IA, Bino-like LSP with Wino-like NLSPs: $M_1 < M_2 < m_{\tilde{t}, \tilde{b}_1} \ll |\mu|$.
- Case IB, Bino-like LSP with Higgsino-like NLSPs: $M_1 < |\mu| < m_{\tilde{t}, \tilde{b}_1} \ll M_2$.

The decays of the light stop or sbottom highly depend on the low-lying neutralino/chargino spectrum, as well as the composition of the light stop and sbottom.

In each scenario, we consider two limiting cases with different stop left-right mixing. In the minimal mixing case, $\tilde{A}_t = A_t - \mu \cot \beta = 0$, the lightest stop mass eigenstate \tilde{t}_1 is either purely \tilde{t}_L ($M_{3SQ} < M_{3SU}$) or purely \tilde{t}_R ($M_{3SQ} > M_{3SU}$). We decouple \tilde{t}_2 for simplicity. In the maximal mixing case with $M_{3SQ} = M_{3SU} = M_{SUSY}$ and $|\tilde{A}_t| = \sqrt{6}M_{SUSY}$, both $\tilde{t}_{1,2}$ are a mixture of \tilde{t}_L and \tilde{t}_R , with mass squared splitting $\Delta m_t^2 \approx 2\sqrt{6}m_t M_{SUSY}$. In our analysis below, we use $\tilde{A}_t > 0$. Negative values of \tilde{A}_t introduce little changes to the numerical results. Since M_{3SQ} also controls the mass for \tilde{b}_L , there is a light $\tilde{b}_1 \sim \tilde{b}_L$ for the light M_{3SQ} case, assuming small sbottom left-right mixing and a decoupled \tilde{b}_R .

The mass spectra for stops and sbottom are shown in Fig. 1. In the minimal mixing case (left panel), $m_{\tilde{t}_L}, m_{\tilde{t}_R}, m_{\tilde{b}_1} \sim M_{3SQ}(M_{3SU})$, especially for large M_{3SQ} (M_{3SU}). In the maximal mixing case (right panel), the mass difference between \tilde{b}_1 and \tilde{t}_1 is typically about 250 GeV while the mass difference between \tilde{t}_2 and \tilde{t}_1 is about 350 GeV or larger.

We used SUSY-HIT [40] to calculate the supersymmetric particle spectrum and decay branching fractions. In this section, unless otherwise specified, we have set the Bino-like

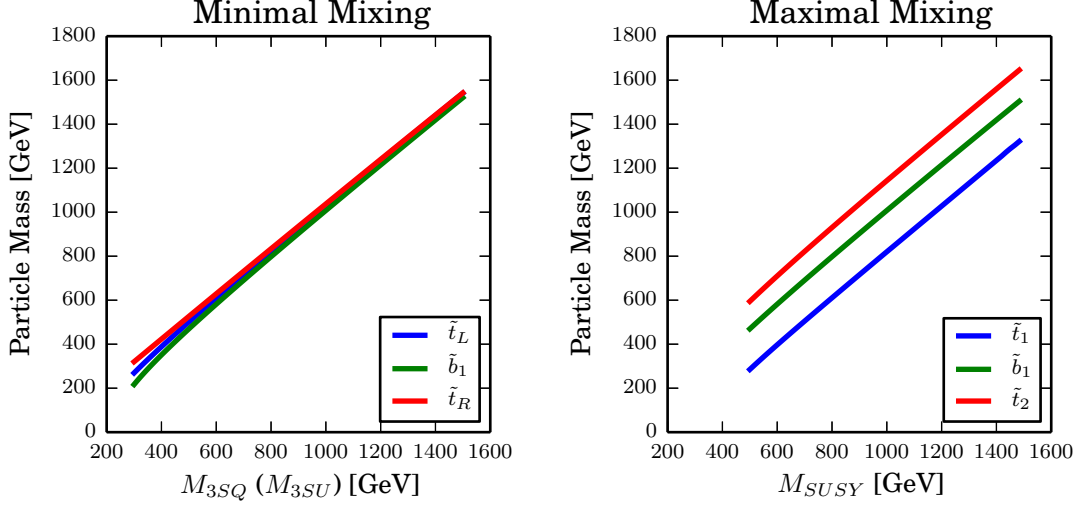


FIG. 1: The mass spectra for stops and sbottom for the minimal mixing case (left panel) and the maximal mixing case with $M_{3SQ} = M_{3SU} = M_{SUSY}$ (right panel).

LSP mass parameter $M_1 = 150$ GeV, the intermediate gaugino mass parameters $M_2, \mu = 300$ GeV in Cases IA and IB, respectively, and $\tan \beta = 10$.

A. Case I: Bino-like LSP with decoupled Wino and Higgsino

The simplest case has a mass spectrum with stop(s), left-handed sbottom, and only the low-lying neutralino being the Bino-like LSP.

In the minimal mixing case with the light stop \tilde{t}_1 as a pure left- or right-handed state, \tilde{t}_1 either directly decays to $t\chi_1^0$ when it is kinematically accessible or through $bW^*\chi_1^0$ with 100% branching fraction. Similarly, in the case of small M_{3SQ} , \tilde{b}_1 decays directly through $b\chi_1^0$ with 100% branching fraction.

In the maximal mixing case, \tilde{t}_1 , \tilde{t}_2 , and \tilde{b}_1 appear in the spectrum, with a typical mass order $m_{\tilde{t}_1} < m_{\tilde{b}_1} < m_{\tilde{t}_2}$ with relatively large mass splittings of 150 GeV or larger. While the decay of \tilde{t}_1 is straightforward (100% into $bW^{(*)}\chi_1^0$), the decays of \tilde{b}_1 and \tilde{t}_2 could have multiple competing channels, as shown in Fig. 2. For \tilde{b}_1 , it dominantly decays into $W\tilde{t}_1$ while the branching fraction of the $\tilde{b}_1 \rightarrow b\chi_1^0$ channel is only about a few percent or less. For \tilde{t}_2 , it dominantly decays into a light stop/sbottom with a gauge boson: $Z\tilde{t}_1$ about 75% and $W\tilde{b}_1$ about 20%. The direct decay down to $t\chi_1^0$ is less than 10%.

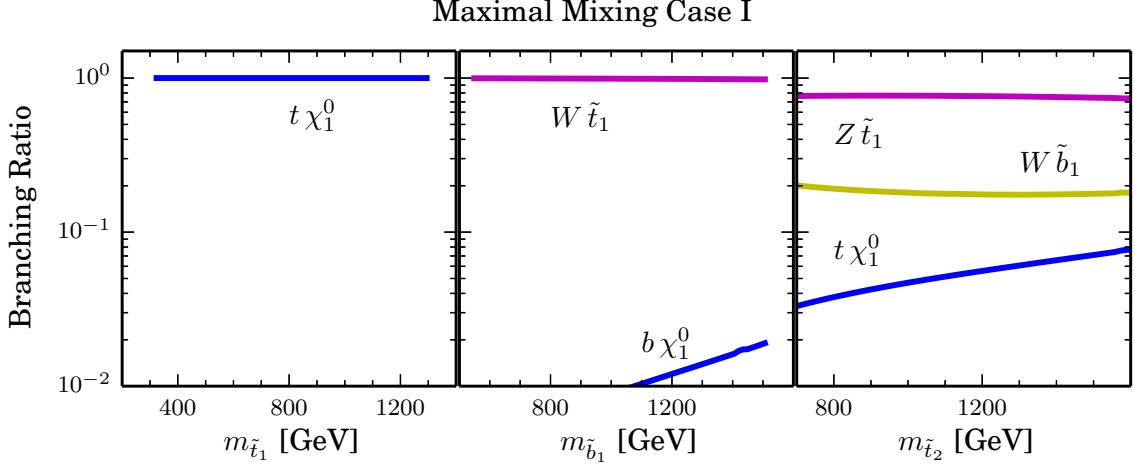


FIG. 2: Branching fractions for \tilde{t}_1 (left), \tilde{b}_1 (middle) and \tilde{t}_2 (right) in the maximal mixing scenario with a Bino-like LSP (Case I). We set $M_1 = 150$ GeV, $M_2 = 2$ TeV, $\mu = 2$ TeV, and $\tan \beta = 10$, which corresponds to $m_{\chi_1^0} = 151$ GeV.

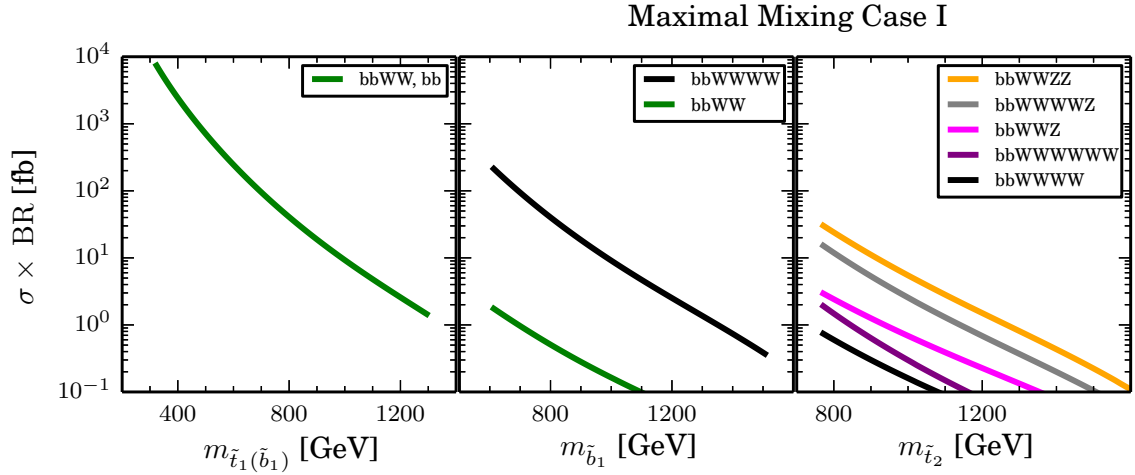


FIG. 3: Case I: left panel shows $\sigma \times \text{BR}$ of final states for \tilde{t}_1 pair production in both the minimal and maximal mixing scenarios, as well as \tilde{b}_1 pair production in the minimal mixing scenario. The middle and right panel show $\sigma \times \text{BR}$ for various final states of \tilde{b}_1 and \tilde{t}_2 pair production, respectively, in the maximal mixing scenario. All channels include \cancel{E}_T in the final states. All the cross sections are for the 14 TeV LHC stop and sbottom pair production, calculated including NLO + NLL corrections [41–43]. The choice of neutralino and chargino mass parameters is the same as in Fig. 2.

The pair production of stops and sbottoms at the LHC, and their subsequent decays result in the appearance of various final states. In the left panel of Fig. 3, we show the $\sigma \times \text{BR}$ of final states $tt/bbWW + \cancel{E}_T$ for \tilde{t}_1 in the minimal and maximal mixing scenarios, as well as $bb + \cancel{E}_T$ for \tilde{b}_1 in the minimal mixing scenario at the 14 TeV LHC. All the cross sections shown in the plots are for stop and sbottom pair production at 14 TeV including NLO supersymmetric QCD correction as well as resummation of soft-gluon emission at next-to-leading logarithmic accuracy [41–43]. Since $\tilde{t}_1 \rightarrow t/bW\chi_1^0$ and $\tilde{b}_1 \rightarrow b\chi_1^0$ dominate in those channels, $\sigma \times \text{BR}$ is the same as the production cross sections for the stop pair and sbottom pair. The middle panel of Fig. 3 shows the $\sigma \times \text{BR}$ for $\tilde{b}_1\tilde{b}_1$ pair production in the maximal mixing scenario. The $bb + \cancel{E}_T$ channel is highly suppressed, while $bbWWWW + \cancel{E}_T$ becomes dominant. The right panel of Fig. 3 shows the $\sigma \times \text{BR}$ for $\tilde{t}_2\tilde{t}_2$ pair production in the maximal mixing scenario. The dominant channel is $ttZZ + \cancel{E}_T$, with $ttWWZ$ being the second dominant channel. The cross section, however, is relatively small, less than about 10 fb for $m_{\tilde{t}_2} \gtrsim 800$ GeV, given the heaviness of the second stop. Note that the range of the stop and sbottom masses are controlled by the choice of parameter $M_{3SQ} = M_{3SU} = M_{SUSY} = 600 \dots 1500$ GeV in the maximal mixing case (see Fig. 1).

B. Case IA: Bino LSP with Wino NLSP

The low lying neutralino/chargino spectrum in Case IA comprises of a Bino-like LSP, as well as a pair of Wino-like states: χ_2^0 and χ_1^\pm with nearly degenerate masses. In the minimal mixing scenario, the decay branching fractions are shown in Fig. 4 for left-handed \tilde{t}_1 (left), \tilde{b}_1 (middle), and right-handed \tilde{t}_1 (right). For the left-handed \tilde{t}_1 , decays to $b\chi_1^\pm$ ($\sim 70\%$ for large $m_{\tilde{t}_1}$) and $t\chi_2^0$ ($\sim 30\%$ for large $m_{\tilde{t}_1}$) dominate over $t\chi_1^0$ once kinematically accessible, due to the stronger $\text{SU}(2)_L$ coupling compared to the relatively weaker $\text{U}(1)_Y$ coupling. Similarly, $\tilde{b}_1 \rightarrow t\chi_1^\pm$ ($\sim 65\%$) and $\tilde{b}_1 \rightarrow b\chi_2^0$ ($\sim 30\%$) dominate over the $b\chi_1^0$ channel for sbottom. Given the dominant decay channels of the Wino-like neutralino/chargino¹: $\chi_1^\pm \rightarrow W\chi_1^0$, $\chi_2^0 \rightarrow Z/h\chi_1^0$, the dominant decay modes for \tilde{t}_1 and \tilde{b}_1 are: $\tilde{t}_1 \rightarrow bW\chi_1^0$, $tZ/h\chi_1^0$, $\tilde{b}_1 \rightarrow tW\chi_1^0$, $bZ/h\chi_1^0$. When \tilde{t}_1 is mostly right-handed, it decays to $t\chi_1^0$ almost 100%, since

¹ For χ_2^0 , whether it decays preferably to $Z\chi_1^0$ or $h\chi_1^0$ depends on the sign of μ , as explained in detail in Ref. [44].

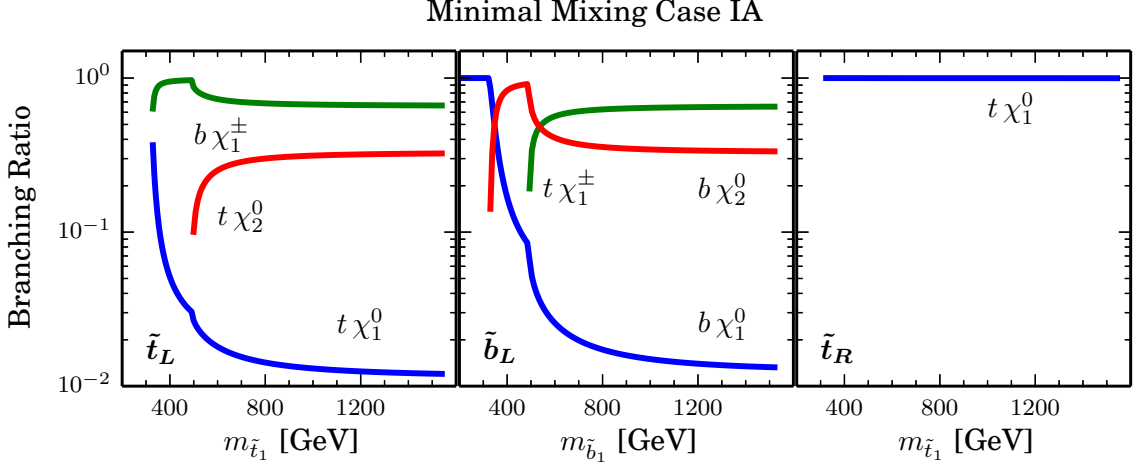


FIG. 4: Case IA: branching fractions for left-handed \tilde{t}_1 (left), \tilde{b}_1 (middle), right-handed \tilde{t}_1 (right) in the minimal mixing scenario. We set $M_1 = 150$ GeV, $M_2 = 300$ GeV, $\mu = 2$ TeV, and $\tan \beta = 10$, which corresponds to $m_{\chi_1^0} = 151$ GeV, $m_{\chi_2^0} = 319$ GeV and $m_{\chi_1^\pm} = 319$ GeV.

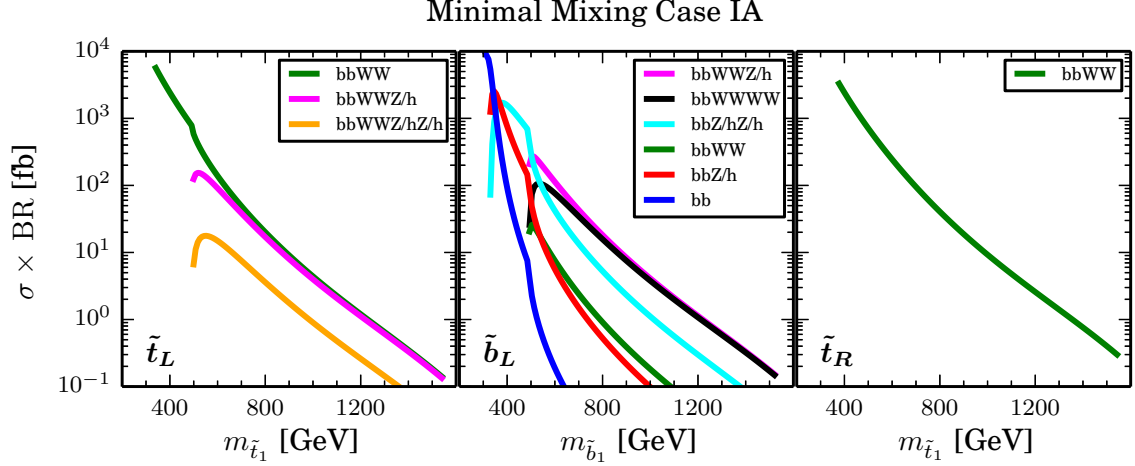


FIG. 5: Case IA: $\sigma \times \text{BR}$ of various final states for pair production of left-handed \tilde{t}_1 (left), \tilde{b}_1 (middle), and right-handed \tilde{t}_1 (right) in the minimal mixing scenario at the 14 TeV LHC. The choice of neutralino and chargino mass parameters is the same as in Fig. 4.

its couplings to the Wino-like neutralino/charginos are highly suppressed.

The left, middle and right panels of Fig. 5 show the $\sigma \times \text{BR}$ for pure left-handed $\tilde{t}_1\tilde{t}_1$, $\tilde{b}_1\tilde{b}_1$ and pure right-handed $\tilde{t}_1\tilde{t}_1$ pair production, respectively, in the minimal mixing scenario

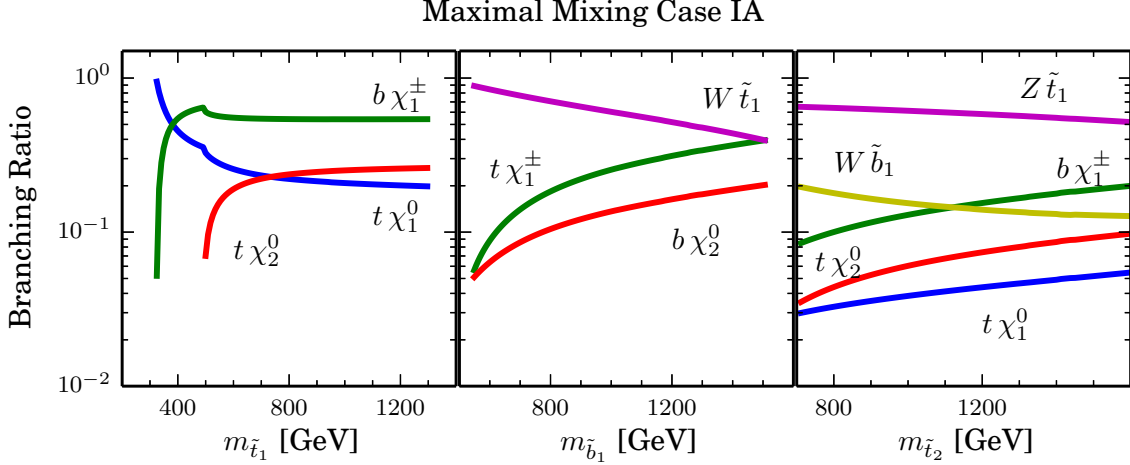


FIG. 6: Case IA: Branching fractions for \tilde{t}_1 (left), \tilde{b}_1 (middle) and \tilde{t}_2 (right) in the maximal mixing scenario. The choice of neutralino and chargino mass parameters is the same as in Fig. 4.

of Case IA. For pure left-handed \tilde{t}_1 , $bbWWZ/h + \cancel{E}_T$ is as abundant as the $bbWW + \cancel{E}_T$ channel, which could be an important new search channel for the stop. For pure left-handed \tilde{b}_1 , the $bb + \cancel{E}_T$ channel is highly suppressed. New final states of $bbWWZ/h$ and $bbWWWW$ are dominant and comparable in size, with $bbZ/hZ/h$ being subdominant, opening up new channels for sbottom searches. The final state for the pure right-handed \tilde{t}_1 is still $bbWW + \cancel{E}_T$, despite the existence of light Wino NLSPs in the spectrum.

For the maximally mixed scenario, the decay of \tilde{t}_1 , \tilde{b}_1 and \tilde{t}_2 are shown in the left, middle and right panels of Fig. 6, respectively. For \tilde{t}_1 with large mass, the decay to $b\chi_1^\pm$, $t\chi_2^0$ still dominates over $t\chi_1^0$, but the corresponding branching fractions are smaller compared to the pure left-handed case (Fig. 4) due to the decrease of the coupling to the Wino-like state caused by the right-handed stop component. For \tilde{b}_1 , while $t\chi_1^\pm$ and $b\chi_2^0$ modes still dominate over $b\chi_1^0$ mode, the new decay channel of $W\tilde{t}_1$ opens up and even dominates over most of the mass range. Its branching fraction varies between 100% to about 40% for $m_{\tilde{b}_1}$ between 600 GeV to 1500 GeV. For \tilde{t}_2 , in addition to $b\chi_1^\pm$ and $t\chi_{1,2}^0$ (about a few percent to 20%), decays to a light stop/sbottom plus a gauge boson [45] become comparable or even dominant: about 50% – 70% for $Z\tilde{t}_1$ and about 20% – 15% for $W\tilde{b}_1$.

The left, middle and right panels of Fig. 7 show the $\sigma \times \text{BR}$ for $\tilde{t}_1\tilde{t}_1$, $\tilde{b}_1\tilde{b}_1$, and $\tilde{t}_2\tilde{t}_2$ respectively for the maximal mixing scenario of Case IA at the 14 TeV LHC. For the

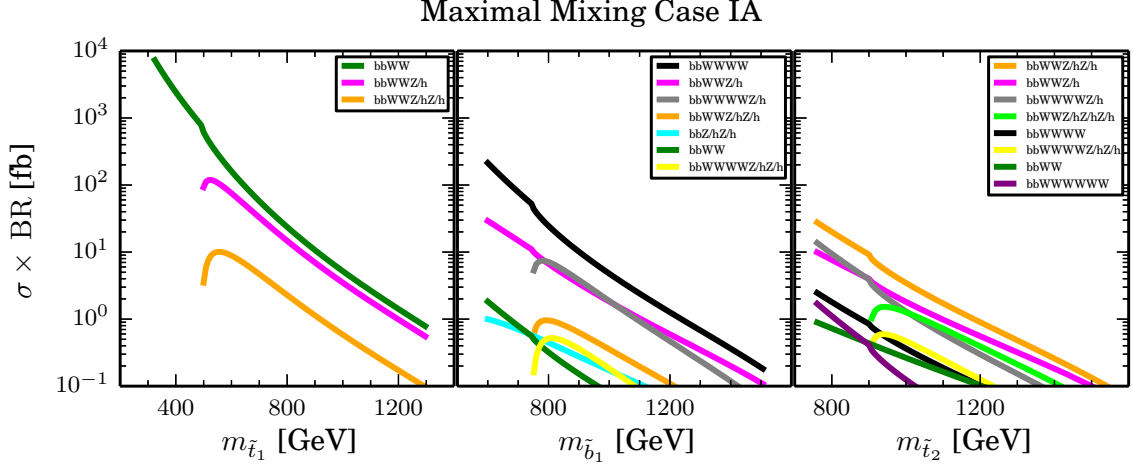


FIG. 7: Case IA: $\sigma \times \text{BR}$ of various final states for pair production of \tilde{t}_1 (left), \tilde{b}_1 (middle), and \tilde{t}_1 (right) in the maximal mixing scenario at the 14 TeV LHC. The choice of neutralino and chargino mass parameters is the same as in Fig. 4.

light stop, while the dominant channel is still $bbWW + \cancel{E}_T$, the subdominant channel $bbWWZ/h + \cancel{E}_T$ could still have a sizable cross section. For the light sbottom, $bbWWWW + \cancel{E}_T$ becomes dominant. For the heavy stop, multiple channels open, with $bbWWZ/hZ/h + \cancel{E}_T$ being dominant, followed by $bbWWZ/h + \cancel{E}_T$, $bbWWWWZ/h + \cancel{E}_T$, and $bbWWZ/hZ/hZ/h + \cancel{E}_T$.

C. Case IB: Bino-LSP with Higgsino-NLSP

The low lying neutralino/chargino spectrum in Case IB comprises of a Bino-like LSP, as well a pair of Higgsino-like neutralino states $\chi_{2,3}^0$ and chargino states χ_1^\pm with nearly degenerate masses. Fig. 8 shows the branching fractions of left-handed \tilde{t}_1 and \tilde{b}_1 and right-handed \tilde{t}_1 in the left, middle and right panels for the minimal mixing scenario. For \tilde{t}_1 , decays to $t\chi_{2,3}^0$ dominate over $b\chi_1^\pm$ and $t\chi_1^0$ since the former ones are controlled by the large top Yukawa coupling, compared to the small bottom Yukawa coupling and $U(1)_Y$ couplings for the latter two. However, for \tilde{b}_1 , the decay of $t\chi_1^\pm$ becomes dominant since the $\tilde{b}_L\tilde{t}_R\tilde{H}_u^+$ coupling is proportional to the top Yukawa while its couplings to $\chi_{2,3}^0$ and χ_1^0 are suppressed by the bottom Yukawa coupling and $U(1)_Y$ couplings. For the right-handed \tilde{t}_1 case, it dominantly decays to $b\chi_1^\pm$, reaching almost 50%, while decays to $t\chi_2^0 + t\chi_3^0$ are about

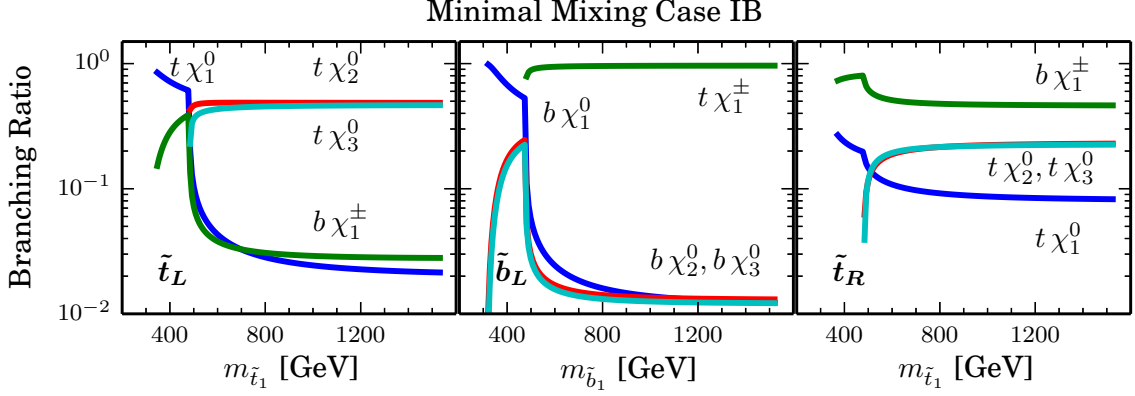


FIG. 8: Case IB: branching fractions for left-handed \tilde{t}_L (left), \tilde{b}_L (middle), right-handed \tilde{t}_R (right) in the minimal mixing scenario. We set $M_1 = 150$ GeV, $\mu = 300$ GeV, $M_2 = 2$ TeV, and $\tan\beta = 10$, which corresponds to $m_{\chi_1^0} = 145$ GeV, $m_{\chi_2^0} = 308$ GeV, $m_{\chi_3^0} = 310$ GeV and $m_{\chi_1^\pm} = 304$ GeV.

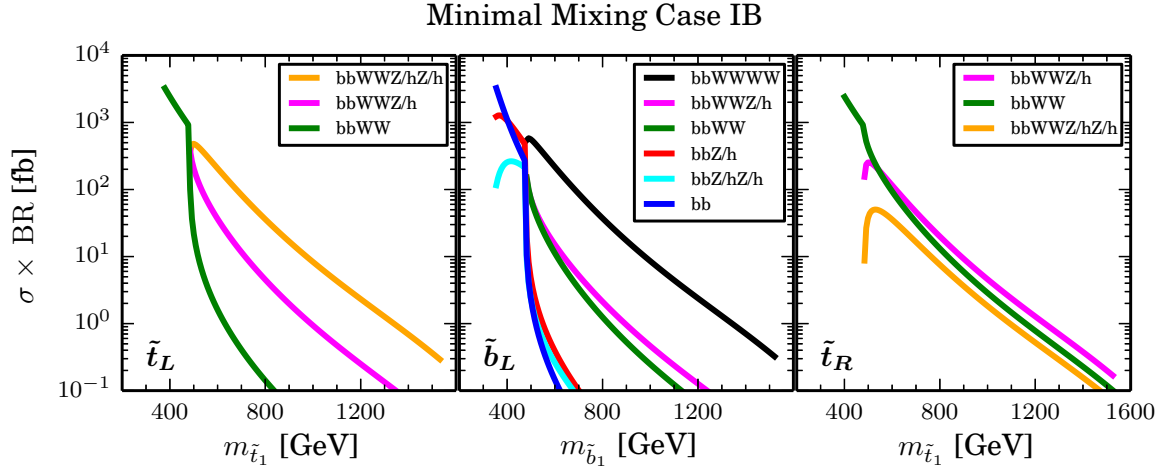


FIG. 9: Case IB: $\sigma \times \text{BR}$ of various final states for pair production of left-handed \tilde{t}_L (left), \tilde{b}_L (middle), and right-handed \tilde{t}_R (right) in the minimal mixing scenario at the 14 TeV LHC. The choice of neutralino and chargino mass parameters is the same as in Fig. 8.

20%. All channels are controlled by the top Yukawa coupling while the latter ones have extra phase space suppression. Given the near degeneracy of the two Higgsino states $\chi_{2,3}^0$, contributions from final states involving $\chi_{2,3}^0$ are usually summed over in collider analyses.

Given the further decays of $\chi_1^\pm \rightarrow W\chi_1^0$, $\chi_{2,3}^0 \rightarrow Z\chi_1^0/h\chi_1^0$ as discussed in detail in [44],

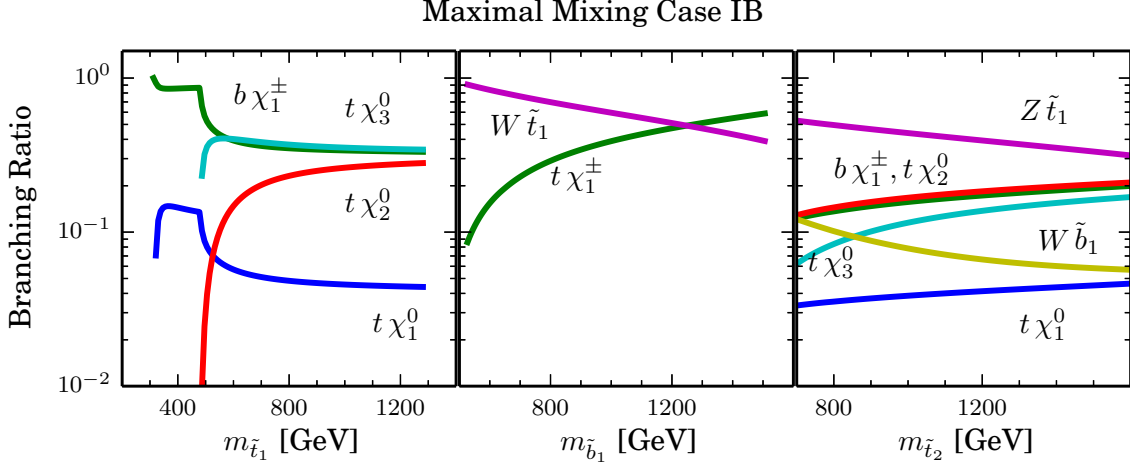


FIG. 10: Case IB: Branching fractions for \tilde{t}_1 (left), \tilde{b}_1 (middle) and \tilde{t}_2 (right) in the maximal mixing scenario. The choice of neutralino and chargino mass parameters is the same as in Fig. 8.

the pair production of stops and sbottoms lead to complicated final states at the collider. The left, middle and right panels of Fig. 9 show the $\sigma \times \text{BR}$ for pure left-handed $\tilde{t}_1\tilde{t}_1$, $\tilde{b}_1\tilde{b}_1$ and pure right-handed $\tilde{t}_1\tilde{t}_1$ pair production in the minimal mixing scenarios of Case IB. For pure left-handed \tilde{t}_1 , $bbWWZ/hZ/h + \cancel{E}_T$ is the dominant final state with the stop search channel $bbWW + \cancel{E}_T$ being highly suppressed. For pure left-handed \tilde{b}_1 , $bbWWWW + \cancel{E}_T$ is the dominant channel. The dominant final states for pure right-handed \tilde{t}_1 are $bbWWZ/h + \cancel{E}_T$ as well as $bbWW + \cancel{E}_T$.

For the maximal mixing scenario, the decay branching fractions for \tilde{t}_1 , \tilde{b}_1 , and \tilde{t}_2 are shown in the left, middle and right panels of Fig. 10, respectively. Since \tilde{t}_1 is an equal mixture of left- and right-handed components, the decays to $t\chi_{2,3}^0$ (dominant for \tilde{t}_L) and $b\chi_1^\pm$ (dominant for \tilde{t}_R) (see the left and right panel of Fig. 8) have roughly the same decay branching fraction, around 30% each. Decay to the final state of $t\chi_1^0$ is typically a few percent, unless other decay modes are kinematically inaccessible at small $m_{\tilde{t}_1}$.

For \tilde{b}_1 , the relative strength of $t\chi_1^\pm$ and $b\chi_{2,3}^0$ is similar to that of the \tilde{b}_1 in the minimal mixing scenario, but the opening of the $W\tilde{t}_1$ mode dominates the decay for most of the mass range, leading to the suppression of the $t\chi_1^\pm$ and $b\chi_{2,3}^0$ modes. With increasing $m_{\tilde{b}_1}$, $t\chi_1^\pm$ becomes more and more important, which dominates over $W\tilde{t}_1$ when $m_{\tilde{b}_1} \gtrsim 1200$ GeV.

For \tilde{t}_2 , decay to $Z\tilde{t}_1$ is dominant, about 60% – 30% for $m_{\tilde{t}_2}$ in the range of 700 –

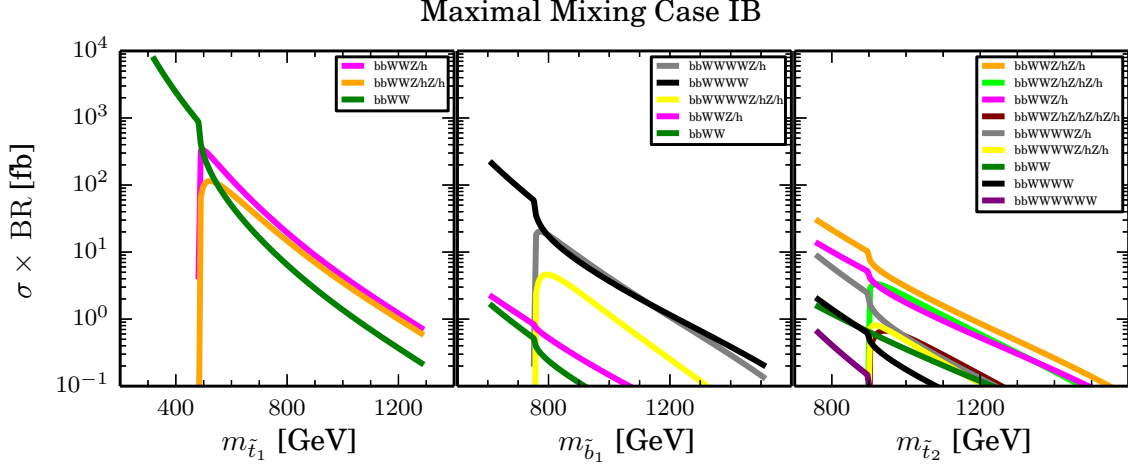


FIG. 11: Case IB: $\sigma \times \text{BR}$ of various final states for pair production of \tilde{t}_1 (left), \tilde{b}_1 (middle), and \tilde{t}_2 (right) in the maximal mixing scenario at the 14 TeV LHC. The choice of neutralino and chargino mass parameters is the same as in Fig. 8.

1600 GeV. Decays to $b\chi_1^\pm$, $t\chi_{2,3}^0$ are sub-dominant, around 10% – 20% for each channel. $\tilde{t}_2 \rightarrow W\tilde{b}_1$ is typically around 10% to about a few percent, while $\tilde{t}_2 \rightarrow t\chi_1^0$ is only at a few percent level.

The left, middle and right panel of Fig. 11 show the $\sigma \times \text{BR}$ for $\tilde{t}_1\tilde{t}_1$, $\tilde{b}_1\tilde{b}_1$, and $\tilde{t}_2\tilde{t}_2$ for the maximal mixing scenario of Case IB at the 14 TeV LHC. For the light stop, the dominant channel is $bbWWZ/h + \cancel{E}_T$, followed by $bbWWZ/hZ/h + \cancel{E}_T$. The $bbWW + \cancel{E}_T$ channel is suppressed by about a factor of 5. For the light sbottom, $bbWWWW + \cancel{E}_T$ and $bbWWWWZ/h + \cancel{E}_T$ are dominant. For the heavy stop, multiple channels open, with $bbWWZ/hZ/h + \cancel{E}_T$ being dominant, followed by $bbWWZ/hZ/hZ/h + \cancel{E}_T$ and $bbWWZ/h + \cancel{E}_T$.

IV. CURRENT COLLIDER SEARCH LIMITS ON STOP AND SBOTTOM

Searches for direct stop and sbottom pair production have been performed at both ATLAS and CMS, with about 20 fb⁻¹ data at $\sqrt{s} = 8$ TeV, and about 5 fb⁻¹ data at $\sqrt{s} = 7$ TeV [5–23]. Here we summarize the current experimental search channels and exclusion bounds assuming a stable neutralino LSP. Stop searches in scenarios with a Gravitino LSP have been analyzed in Refs. [13, 16].

- $\tilde{t}_1 \rightarrow t^{(*)}\chi_1^0$ and $\tilde{t}_1 \rightarrow b\chi_1^\pm \rightarrow bW^{(*)}\chi_1^0$ [5–10]

ATLAS results on fully hadronic final states [5] exclude stops in the regions of $270 < m_{\tilde{t}_1} < 645$ GeV for $m_{\tilde{\chi}_1^0} < 30$ GeV, assuming both stops decay 100% via $\tilde{t}_1 \rightarrow t\chi_1^0$. Regions of $245 < m_{\tilde{t}_1} < 400$ GeV for $m_{\tilde{\chi}_1^0} < 60$ GeV, $m_{\chi_1^\pm} = 2m_{\chi_1^0}$ are excluded when both stops decay 100% via $\tilde{t}_1 \rightarrow bW^{(*)}\chi_1^0$. For $\text{BR}(\tilde{t}_1 \rightarrow bW^{(*)}\chi_1^0) = \text{BR}(\tilde{t}_1 \rightarrow t\chi_1^0) = 50\%$, stop masses in the range of 250 – 550 GeV are excluded for $m_{\tilde{\chi}_1^0} < 60$ GeV, $m_{\chi_1^\pm} = 2m_{\chi_1^0}$.

For semileptonic channels, stop masses between 210 GeV and 640 GeV are excluded at 95% C.L. for a massless LSP, and stop masses around 550 GeV are excluded for LSP mass below 230 GeV [6], assuming $\text{BR}(\tilde{t}_1 \rightarrow t\chi_1^0) = 100\%$. For $\text{BR}(\tilde{t}_1 \rightarrow b\chi_1^\pm \rightarrow bW^{(*)}\chi_1^0) = 100\%$, the excluded stop and LSP masses depend strongly on the mass of the χ_1^\pm . For $m_{\chi_1^\pm} = 2m_{\chi_1^0}$, stop masses up to 500 GeV are excluded for LSP masses in the range of 100 and 150 GeV. For the compressed spectrum case when $m_{\chi_1^\pm} - m_{\chi_1^0}$ is small with soft leptons from χ_1^\pm decay, stop masses between 265 (240) GeV and 600 GeV are excluded for $m_{\chi_1^\pm} - m_{\chi_1^0} = 5(20)$ GeV with an LSP mass of 100 GeV. For small mass splitting between \tilde{t}_1 and χ_1^\pm (for example, 10 GeV) with soft b jets, stop masses below 390 GeV are excluded for a massless LSP. When both decay modes $\tilde{t}_1 \rightarrow t\chi_1^0$ and $\tilde{t}_1 \rightarrow b\chi_1^\pm$ are open, the excluded stop masses increase from 530 GeV to 660 GeV for an LSP mass of 100 GeV when $\text{BR}(\tilde{t}_1 \rightarrow t\chi_1^0)$ is increased from 0% to 100% and $m_{\chi_1^\pm} = 2m_{\chi_1^0}$. The limits get weaker with an increased branching ratio to decays other than $\tilde{t}_1 \rightarrow t\chi_1^0$ and $\tilde{t}_1 \rightarrow b\chi_1^\pm$.

Limits from the pure leptonic channels are weaker [7]. Stops with masses between 215 GeV and 530 GeV decaying to an on-shell t -quark and a neutralino are excluded at 95% C. L. for a 1 GeV neutralino. For $m_b + m_W + m_{\chi_1^0} < m_{\tilde{t}_1} < m_t + m_{\chi_1^0}$ with an off-shell top and a neutralino LSP, the stop masses are excluded between 90 GeV and 170 GeV. For $\text{BR}(\tilde{t}_1 \rightarrow b\chi_1^\pm) = 100\%$, the limits on the stop mass depend on both the LSP mass and $m_{\chi_1^\pm}$. $m_{\tilde{t}_1}$ between 150 GeV and 445 GeV is excluded at 95% C. L. for $m_{\tilde{t}_1} = m_{\chi_1^\pm} + 10$ GeV, in the case of a 1 GeV neutralino LSP. For $m_{\tilde{t}_1} = 2m_{\chi_1^\pm}$, stop masses between 210 GeV and 340 GeV are excluded for an LSP mass of 100 GeV. For a fixed $m_{\chi_1^\pm} = 106$ GeV, stop masses between 240 GeV to 325 GeV are excluded with an LSP mass of 1 GeV.

Limits from CMS are very similar [8–10]. Note that limits on the stop exclusion depend on the branching fractions of $\tilde{t}_1 \rightarrow t^{(*)}\chi_1^0$ and $\tilde{t}_1 \rightarrow b\chi_1^\pm$. For $\tilde{t}_1 \rightarrow b\chi_1^\pm$, the limits also depend on the mass of the intermediate chargino.

- $\tilde{t}_1 \rightarrow c\chi_1^0$ or $\tilde{t}_1 \rightarrow bff'\chi_1^0$ [11, 12]

For small mass splitting between $m_{\tilde{t}_1}$ and $m_{\chi_1^0}$, stop decays via $\tilde{t}_1 \rightarrow c\chi_1^0$ or $\tilde{t}_1 \rightarrow bff'\chi_1^0$ [11, 12]. For 100% branching fraction of $\tilde{t}_1 \rightarrow c\chi_1^0$, searches on charm tagged events and monojet-like events exclude stop masses around 240 GeV for $\Delta m = m_{\tilde{t}_1} - m_{\chi_1^0} < 85$ GeV. Stop masses up to 270 GeV are excluded for an LSP mass of 200 GeV. For nearly degenerate stop and LSP, stop masses up to about 260 GeV are excluded. For 100% branching fraction of $\tilde{t}_1 \rightarrow bff'\chi_1^0$, searches based on monojet plus \cancel{E}_T exclude stop masses up to about 255 GeV for $\Delta m \sim m_b$ and about 150 (200) GeV for $m_b < \Delta m < 50(35)$ GeV.

For small mass splitting between $m_{\chi_1^\pm}$ and $m_{\chi_1^0}$ with undetectable decay products of χ_1^\pm , pair production of stop with $\tilde{t}_1 \rightarrow b\chi_1^\pm$ leads to two b jets plus \cancel{E}_T events. Results from ATLAS [17] exclude stop masses up to 580 (440) GeV for $m_{\chi_1^\pm} - m_{\chi_1^0} = 5(20)$ GeV and $m_{\chi_1^0} = 100$ GeV.

- $\tilde{t}_2 \rightarrow \tilde{t}_1 Z/h$ [13–15]

Searches for the second stop utilize the decay of $\tilde{t}_2 \rightarrow \tilde{t}_1 Z/h$, looking for signals including b -jets and large \cancel{E}_T with either same flavor leptons reconstruction of the Z boson [13] and/or high p_T jet and b -jet multiplicities with additional leptons [14, 15]. The interpretation is performed in the region $m_{\tilde{t}_1} - m_{\chi_1^0} \sim m_t$, which is hard to probe by $\tilde{t}_1 \rightarrow t\chi_1^0$ channel given the relative small \cancel{E}_T . For $\text{BR}(\tilde{t}_2 \rightarrow \tilde{t}_1 Z) = 100\%$, the second stop mass is excluded up to about 600 GeV for a light LSP mass. For $\text{BR}(\tilde{t}_2 \rightarrow \tilde{t}_1 h) = 100\%$, the second stop mass exclusion limit is about 540 GeV. When the decay branching fraction to $\tilde{t}_1 Z$ and $\tilde{t}_1 h$ is 50% each, the exclusion limit is about 580 GeV for a light LSP mass.

- $\tilde{b}_1 \rightarrow b\chi_1^0$ [11, 17, 18]

Sbottom pair production with $\tilde{b}_1 \rightarrow b\chi_1^0$ leads to signals with two b jets and large \cancel{E}_T . The null results from ATLAS [17] exclude sbottom masses up to 620 GeV for $m_{\chi_1^0} < 120$ GeV. $m_{\tilde{b}_1} - m_{\chi_1^0}$ is excluded up to 50 GeV for sbottom masses up to 300

GeV. The exclusion limits depend sensitively on the branching fraction of $\tilde{b}_1 \rightarrow b\chi_1^0$. For 60% branching fractions, the sbottom exclusion limit is reduced to 520 GeV. The CMS exclusion limits are about 70 GeV stronger [18]. For small mass splitting between sbottom and the LSP: $m_{\tilde{b}_1} - m_{\chi_1^0} \sim m_b$, monojet plus \cancel{E}_T search excludes sbottom masses up to about 255 GeV [11].

- $\tilde{b}_1 \rightarrow b\chi_2^0$ [19, 20]

Sbottom searches on direct sbottom pair production with $\tilde{b}_1 \rightarrow b\chi_2^0$ with 100% decay branching fraction of $\chi_2^0 \rightarrow \chi_1^0 h$ have been performed at ATLAS [19], searching for signals with zero lepton, large \cancel{E}_T , high jet multiplicity and at least three b -tagged jets. Null search results exclude the sbottom masses between 340 and 600 GeV for $m_{\chi_2^0} = 300$ GeV and $m_{\chi_1^0} = 60$ GeV. No sensitivity is obtained for $m_{\chi_2^0} < 240$ GeV due to the soft \cancel{E}_T in the signal events. For $\tilde{b}_1 \rightarrow b\chi_2^0$ with 100% decay branching fraction of $\chi_2^0 \rightarrow \chi_1^0 Z$, three leptons plus one b jet plus \cancel{E}_T search at the CMS excludes sbottom masses up to 450 GeV for LSP masses between 100 to 125 GeV and $m_{\chi_1^\pm} - m_{\chi_1^0} = 110$ GeV [20].

- $\tilde{b}_1 \rightarrow t\chi_1^\pm$ [20–23]

Sbottom searches on direct sbottom pair production with $\tilde{b}_1 \rightarrow t\chi_1^\pm$ with 100% decay branching fraction of $\chi_1^\pm \rightarrow W\chi_1^0$ have been performed at both ATLAS and CMS [21, 22], looking for signals with two same charge leptons or three leptons plus multiple jets. The interpretation was done for fixed $m_{\chi_1^0} = 60$ GeV as well as varying $m_{\chi_1^0}$ with $m_{\chi_1^\pm} = 2m_{\chi_1^0}$. The sbottom mass limit is about 440 GeV in both cases for $m_{\chi_1^\pm} < m_{\tilde{b}_1} - m_t$ [21]. The CMS limits are about 50 to 100 GeV stronger [20, 22, 23].

At the 14 TeV LHC, with the dominant decay channel of $\tilde{t}_1 \rightarrow t\chi_1^0$, studies using semileptonic channel and fully hadronic channel show that for LSP masses below 200 GeV, a 5σ reach of stop discovery is possible for stop masses up to about 1 TeV with 300 fb^{-1} integrated luminosity [46]. For the high luminosity option of LHC (HL-LHC) with 3000 fb^{-1} integrated luminosity, the discovery reach is extended by about 200 GeV. The 95% exclusion limit is about 1.2 TeV (1.45 TeV) with 300 (3000) fb^{-1} integrated luminosity. For sbottom searches with $\tilde{b}_1 \rightarrow b\chi_1^0$, the discovery reach is about 1.1 (1.3) TeV and the

exclusion reach is about 1.4 (1.55) TeV with 300 (3000) fb^{-1} integrated luminosity [47]. CMS analyses using specific full spectrum benchmark points show similar sensitivities [48].

V. COLLIDER ANALYSIS

Given a different neutralino/chargino mass spectrum, many new decay channels for stop and sbottom appear, while the channels of $\tilde{t}_1 \rightarrow t\chi_1^0, b\chi_1^\pm$ and $\tilde{b}_1 \rightarrow b\chi_1^0$ could be highly suppressed. This leads to the relaxation of current collider search limits based on those above mentioned channels. At the same time, those new channels provide new discovery opportunities. To demonstrate the new discovery potential, we pick one particular channel as our benchmark scenario for collider analyses. Studies on other possible mass spectrum and decay channels are left for future study.

In this section, we study the detectability of the light stop in Case IA with a mass hierarchy of $M_1 < M_2 < M_{3SQ} \ll |\mu|, M_{3SU}$, resulting in a mass spectrum including a mostly left-handed stop and mostly left-handed sbottom, Wino-like NLSPs, and a Bino-like LSP. In our analyses, we consider the kinematic region of $m_{\tilde{t}_1} - m_{\chi_2^0} > m_t$ and $m_{\chi_2^0} - m_{\chi_1^0} > m_h$ such that $\tilde{t}_1 \rightarrow t\chi_2^0$ and $\chi_2^0 \rightarrow h\chi_1^0$ are kinematically open. The collider analyses of the current event topology can not be applied for the more compressed scenarios when either M_{3SQ} is close to M_2 or M_2 is close to M_1 . To illustrate the decay branching fractions, we choose a benchmark point with the specific set of parameters and the corresponding mass spectrum shown in Table I. The value of \tilde{A}_t is chosen such that the SM-like Higgs mass is around 125 GeV. Note that even though \tilde{A}_t is set to a large value, the large mass splitting between M_{3SQ} and M_{3SU} results in a mostly left-handed \tilde{t}_1 and mostly right-handed \tilde{t}_2 . Therefore, the decay patterns of \tilde{t}_1 and \tilde{b}_1 follow those of the Case IA: purely left-handed stop/sbottom in the minimal mixing scenario.

M_1	M_2	μ	\tilde{A}_t	M_{3SQ}	M_{3SU}	χ_1^0	χ_2^0	χ_1^\pm	\tilde{t}_1	h	\tilde{b}_1
150	300	2000	2750	650	2000	151	319	319	646	125	637

TABLE I: Mass parameters and mass spectrum of SUSY particles for the benchmark point. All masses are in units of GeV.

The decay channels for the light stop of the benchmark point are shown in Table II. While the dominant decay channel is $\tilde{t}_1 \rightarrow b\chi_1^+$ with 71% branching fraction, the subdom-

inant channel $\tilde{t}_1 \rightarrow t\chi_2^0$ is about 27%, providing an interesting signal where χ_2^0 can either decay to a Higgs or a Z boson. For our choice of parameters with $\mu > 0$, χ_2^0 dominantly decays to $h\chi_1^0$, as shown in Table II. Flipping the sign of μ could lead to another interesting channel of $\chi_2^0 \rightarrow Z\chi_1^0$, which is left for future study.

Decay	Branching Fraction	Decay	Branching Fraction
$\tilde{t}_1 \rightarrow t\chi_1^0$	2%	$\chi_2^0 \rightarrow Z\chi_1^0$	3%
$\tilde{t}_1 \rightarrow t\chi_2^0$	27%	$\chi_2^0 \rightarrow h\chi_1^0$	97%
$\tilde{t}_1 \rightarrow b\chi_1^+$	71%	$\chi_1^+ \rightarrow W^+\chi_1^0$	100%

TABLE II: Decay branching fractions of \tilde{t}_1 , χ_2^0 and χ_1^+ for the benchmark point.

For our benchmark point with the reduced branching fraction of $\text{BR}(\tilde{t}_1 \rightarrow b\chi_1^\pm) = 71\%$, the current collider search limits on the stop are much more relaxed: less than about 500 GeV for $m_{\tilde{t}_1}$. However, new search channels open up, which play a complementary role for stop searches at the LHC.

In our analysis, we study the stop pair production with mixed stop decay final states of $\tilde{t}_1 \rightarrow t\chi_2^0 \rightarrow th\chi_1^0$, $\tilde{t}_1 \rightarrow b\chi_1^\pm \rightarrow bW\chi_1^0$. The branching fraction for such decay is about 38% for our benchmark point and varies between 25% and 50% for a stop mass larger than 500 GeV with $M_2 = M_1 + 150$ GeV. We consider semileptonic decays of the two W s and the Higgs decay to two b -quarks. Since we choose the CP-odd Higgs mass m_A to be 2000 GeV, we are in the decoupling region of the Higgs sector with the light CP-even Higgs being SM-like. Given that we are in the Bino-LSP scenario with $M_2 = M_1 + 150$ GeV, additional possible decay modes of h into neutralino/charginos are either highly suppressed or kinematically forbidden. Therefore, the light CP-even Higgs is consistent with the observed signal of a 125 GeV SM-like Higgs boson. In our analyses, we have taken the branching fraction of $h \rightarrow b\bar{b}$ to be the SM value of 57.7%. The signal contains four b -jets, two jets, one isolated lepton and large missing energy. The presence of a single lepton helps to reduce QCD multijets backgrounds without significant branching fraction suppression.

The dominant SM backgrounds are $b\bar{b}WW$ (dominantly from $t\bar{t}$) and $t\bar{t}b\bar{b}$. While $t\bar{t}h$ is an irreducible background, the production cross section is typically small. Other backgrounds consist of $t\bar{t}W$ and $t\bar{t}Z$.

Event samples are generated using Madgraph MG5_aMC_V2_2_1 [49], processed through Pythia 6.420 [50] for fragmentation and hadronization and then through Delphes-3.1.2 [51] with the Snowmass combined LHC detector card [52] for detector simulation. Both the SM backgrounds and the stop pair production signal are normalized to theoretical cross sections, calculated including higher-order QCD corrections [41–43, 53–57]. For event generation, we have set m_t to be 173 GeV, and the Higgs mass m_h to be 125 GeV. The renormalization scale and factorization scale are taken to be $\sqrt{M^2 + p_T^2}$ for a single heavy particle. For pair production of heavy particles, the geometric mean of $\sqrt{M^2 + p_T^2}$ for each particle is used. For the signal process, we scan the parameter range of $M_{3SQ} = 400 \dots 1100$ GeV with step size of 25 GeV, and $M_1 = 3 \dots 750$ GeV with step size of 25 GeV. We fix M_2 to be $M_2 = M_1 + 150$ GeV.

We apply the following basic event selection cuts:

- Events are required to have at least four isolated jets² with

$$p_T^{j1,j2,j3} > 40 \text{ GeV}, p_T^{j4} > 25 \text{ GeV}, |\eta^j| < 2.5. \quad (7)$$

All isolated jets satisfying $p_T^j > 25 \text{ GeV}$, $|\eta^j| < 2.5$ are counted in N_j .

- Among the jets, at least two are b -tagged jets. The b -tagging efficiency depends on the p_T and η of the jets, which is 0 for $p_T < 15 \text{ GeV}$ or $|\eta| > 2.5$, about 70% for $|\eta^j| < 1.2$ and about 60% for $1.2 < |\eta^j| < 2.5$ with $p_T^j \gtrsim 200 \text{ GeV}$. The mistag rate depends on the quark species, as well as p_T and η of the jets. It is about 15% for c -quark and a constant 2% for light jets.
- One isolated lepton³ (e or μ) is required to have

$$p_T^\ell > 20 \text{ GeV with } |\eta^\ell| < 2.5. \quad (8)$$

Additional optimization selection cuts are applied to further enhance the signal and suppress the SM backgrounds:

² The anti- k_t jet algorithm is used in the reconstruction of jets, with the jet radius being 0.5. For isolated jets, we require any jet within $\Delta R = 0.2$ of a lepton be discarded. An event is discarded if the distance between \cancel{E}_T and all jets, $\Delta\Phi(\cancel{E}_T, j)$, is less than 0.8.

³ For an isolated lepton, we require $\Delta R(\ell, j) > 0.4$.

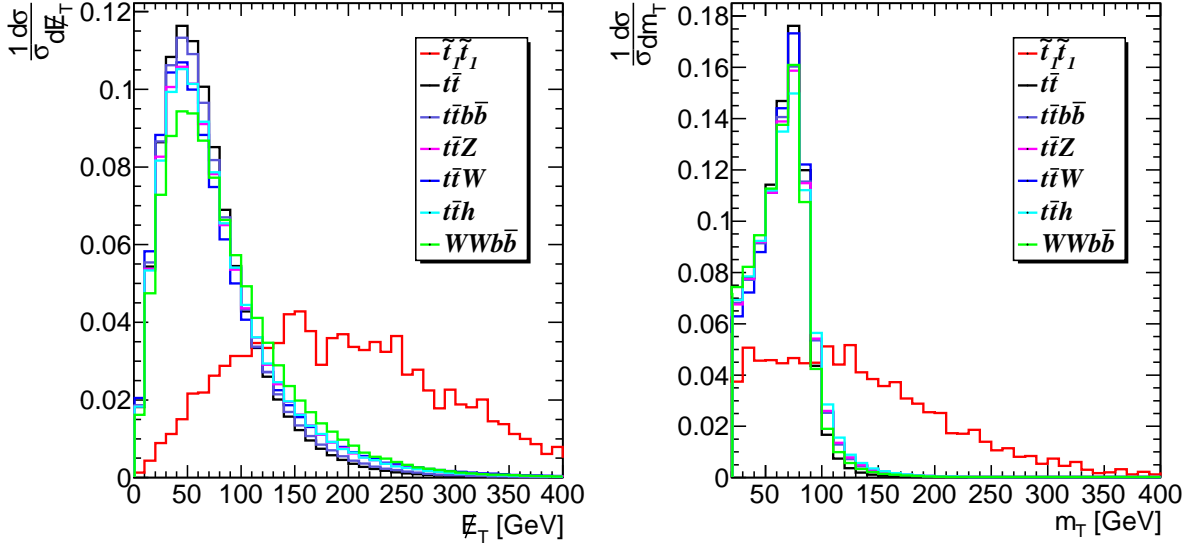


FIG. 12: The distribution of \cancel{E}_T (left) and m_T (right) for the signal at the benchmark point and the SM backgrounds after basic selection cuts.

- \cancel{E}_T , defined as the magnitude of the missing transverse momentum, \mathbf{p}_T^{miss} , to be above 100, 120, 140, 160, 180, and 200 GeV.
- H_T , defined as the scalar sum of the p_T of all surviving isolated jets satisfying $p_T^j > 25$ GeV, $|\eta^j| < 2.5$: $H_T = \sum p_T^{jet}$, to be above 400, 450, 500, 550, 600 GeV.
- Transverse mass m_T , defined as the invariant mass of the lepton and the missing transverse momentum:

$$m_T = \sqrt{2p_T^\ell \cancel{E}_T (1 - \cos \phi(\mathbf{p}_T^\ell, \mathbf{p}_T^{miss}))}, \quad (9)$$

to be above 100, 120, 140, 160, 180, 200 GeV.

- N_j , the number of all surviving isolated jets satisfying $p_T^j > 25$ GeV and $|\eta^j| < 2.5$, to be at least 4, 5, or 6.
- N_{bj} , the number of all tagged b -jets, to be at least 2, 3, or 4.

The distributions of \cancel{E}_T and m_T for both the signal and the SM backgrounds are shown in Fig. 12. In the \cancel{E}_T distribution, the \cancel{E}_T for all the SM backgrounds comes only from the neutrino, which is typically smaller than that of the signal with additional \cancel{E}_T contribution

from the LSP. The transverse mass for the signal process extends beyond the SM threshold of the W boson mass. The H_T distribution of the signal is maximum at a higher value compared to the SM backgrounds.

In Table III, we present the cumulative cut efficiencies for the signal and dominant SM backgrounds with one set of selection cuts. By utilizing strong \cancel{E}_T , H_T and m_T selection cuts, we significantly reduce the SM backgrounds. The stop signal process typically generates multiple hard jets in our specified decay. The N_{bj} cut further plays an important role in cutting $t\bar{t}$, $t\bar{t}W$, and $t\bar{t}Z$ backgrounds. $t\bar{t}$ is the dominant background given its large cross section. The tails in the $t\bar{t}$ missing E_T and H_T distribution are more relevant than those of the rare SM processes of $t\bar{t}Z/W$. $t\bar{t}b\bar{b}$ is the second dominant background given its relatively large cross section and similar final states to the signal process. $t\bar{t}h$, $t\bar{t}Z$, and $t\bar{t}W$ can be sufficiently suppressed due to low cross sections. We impose a constraint on the number of signal events, $N_s \geq 3$ for 300 fb^{-1} in order to obtain sufficient statistics.

Description	$\tilde{t}_1\tilde{t}_1$	$t\bar{t}$	$t\bar{t}b\bar{b}$	$t\bar{t}h$	$t\bar{t}Z$	$t\bar{t}W$
CS (fb)	10	261230	2346	108	221	218
Basic selections	39%	14%	24%	31%	30%	25%
$\cancel{E}_T > 200 \text{ GeV}$	18.5%	0.23%	0.58%	1.2%	1.2%	1.2%
$H_T > 500 \text{ GeV}$	15.6%	7.4×10^{-4}	0.29%	0.78%	0.77%	0.69%
$m_T > 160 \text{ GeV}$	5.9%	1.8×10^{-6}	3.6×10^{-5}	6.6×10^{-5}	7.0×10^{-5}	6.0×10^{-5}
$N_j \geq 5$	4.4%	8.5×10^{-7}	2.1×10^{-5}	3.7×10^{-5}	3.8×10^{-5}	2.6×10^{-5}
$N_{bj} \geq 2$	2.9%	2.9×10^{-7}	1.1×10^{-5}	2.2×10^{-5}	1.1×10^{-5}	7.6×10^{-6}
CS (fb) after selection cuts	0.29	0.075	0.026	0.0023	0.0025	0.0017

TABLE III: The cumulative cut efficiencies for the signal at the benchmark point and all SM backgrounds. The cross sections shown in the second row are for the semileptonic final states.

In Fig. 13, we show the 95% C.L. exclusion limit and 5σ reach in the parameter space of $m_{\tilde{t}_1}$ versus $m_{\chi_1^0}$ for the 14 TeV LHC with 300 fb^{-1} luminosity. M_2 is fixed to be $M_1 + 150 \text{ GeV}$ and 10% (30%) systematic uncertainties on SM backgrounds are assumed for solid (dotted) curves. For each mass point of $(m_{\tilde{t}_1}, m_{\chi_1^0})$, given the mass dependence of the production cross section and decay branching fractions, the signal $\sigma \times \text{BR}$ for each individual point has been used. All combinations of the cut values for the advanced selection cuts of

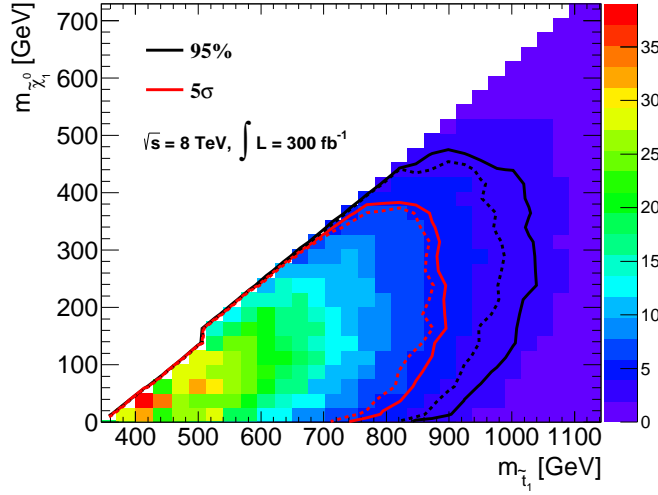


FIG. 13: The plot shows the 5σ discovery reach (red) and 95% exclusion limits (black) of the stop in the $m_{\tilde{t}_1} - m_{\chi_1^0}$ plane for 14 TeV LHC with 300 fb^{-1} of integrated luminosity. M_2 is fixed to be $M_1 + 150 \text{ GeV}$ and 10% (30%) systematic uncertainties are assumed for solid (dotted) curves. The color coding on the right indicates the signal significance defined simply as S/\sqrt{B} to guide the eye. For exclusion and discovery reach, we used the signal significance defined as $S/\sqrt{S+B+(\epsilon \times B)^2}$ and $S/\sqrt{B+(\epsilon \times B)^2}$, respectively. Here ϵ is the assumed systematic uncertainty.

\cancel{E}_T , H_T , m_T , N_j and N_{bj} are examined. The optimized combination that gives the best significance is used for that particular mass point. For the 5σ reach, stop masses up to 740 GeV can be reached for a massless LSP and about 940 GeV with $m_{\chi_1^0} = 250 \text{ GeV}$, assuming 10% systematic uncertainties. The 95% C.L. exclusion limits are about 840 GeV for stops with a light χ_1^0 , while the reach is 1040 GeV for $m_{\chi_1^0} = 250 \text{ GeV}$. Limits with 30% systematic uncertainties are about 50 GeV worse.

Note that a light left-handed sbottom with mixed decay of $\tilde{b}_1 \rightarrow b\chi_2^0$ and $\tilde{b}_1 \rightarrow t\chi_1^\pm$ could lead to the same final states. We focused on the stop search sensitivities in the current study. Collider studies for the sbottom search as well as the combined reach in M_{3SQ} versus $m_{\chi_1^0}$ plane can be found in Ref. [58].

VI. SUMMARY AND CONCLUSION

Most of the current stop and sbottom searches at the LHC have been performed considering the channels of $tt + \cancel{E}_T$, $bbWW + \cancel{E}_T$ for stop and $bb + \cancel{E}_T$ for sbottom, assuming the stop and sbottom decay 100% into these channels. However, in many regions of MSSM parameter space, these decay channels are subdominant, resulting in relaxed bounds from current LHC searches. In this work, we studied decays of the stop and sbottom in the cases of a Bino-like LSP with either Wino-like or Higgsino-like NLSPs in the low energy spectrum, for the left- and right-handed stops and left-handed sbottom in the minimal mixing scenario, and $\tilde{t}_{1,2}$, \tilde{b}_1 in the maximal mixing scenario. We found that new decay channels of $\tilde{t}_1 \rightarrow t\chi_{2,3}^0$, $\tilde{b}_1 \rightarrow b\chi_{2,3}^0, t\chi_1^\pm, W\tilde{t}_1$ open up, which could even dominate over $\tilde{t}_1 \rightarrow t\chi_1^0, b\chi_1^\pm$ and $\tilde{b}_1 \rightarrow b\chi_1^0$ channels. For the heavier stop state, \tilde{t}_2 , a new channel of $\tilde{t}_2 \rightarrow W\tilde{b}_1$ appears in addition to $\tilde{t}_2 \rightarrow Z\tilde{t}_1$ in the maximal mixing scenario. Given the further decays of $\chi_{2,3}^0$ and χ_1^\pm , pair production of stops and sbottoms at the LHC typically leads to bb plus multiple gauge bosons plus \cancel{E}_T final states. Current search channels of $bbWW + \cancel{E}_T$ and $bb + \cancel{E}_T$ could be highly suppressed.

We performed a sample collider analysis for the reach of the stop at the 14 TeV LHC with 300 fb^{-1} integrated luminosity for one particularly interesting channel in the Bino-like LSP with Wino-like NLSP case. We considered left-handed stop pair production mixed stop decay final states of $\tilde{t}_1 \rightarrow t\chi_2^0 \rightarrow th\chi_1^0$, $\tilde{t}_1 \rightarrow b\chi_1^\pm \rightarrow bW\chi_1^0$, leading to the $bbbbjj\ell + \cancel{E}_T$ collider signature. The branching fraction for such decay varies between 25% and 50% for a stop mass larger than 500 GeV with $M_2 = M_1 + 150 \text{ GeV}$. Our results show that for a LSP mass of 250 GeV, the 95% C.L. exclusion reach is about 1040 GeV for the stop and the 5σ reach is about 940 GeV, assuming 10% systematic uncertainties. The reach decreases with smaller LSP mass.

Considering different low-lying neutralino/chargino spectra provides several promising channels for the stop and sbottom study. In this paper we focused on final states with a Higgs boson. Decays of χ_2^0 to $Z\chi_1^0$ could be dominant with a different choice of $\text{sign}(\mu)$. Furthermore, a different mass spectrum of neutralino/chargino with LSP being either Wino-like or Higgsino-like might give rise to more interesting final states. It is important to identify the leading decay channels in various regions of parameter space to fully explore the reach of the LHC for the third generation squarks, which has important implications

for the stabilization of the electroweak scale in supersymmetric models. The strategy developed in our analysis can be applied to the study of top partners in other new physics scenarios as well.

Acknowledgments

We would like to thank Felix Kling, Tao Han, Yongcheng Wu, Bing Zhang for helpful discussions. The work is supported by the Department of Energy under Grant DE-FG02-04ER-41298. This work was supported in part by National Science Foundation Grant No. PHYS-1066293 and the hospitality of the Aspen Center for Physics.

-
- [1] G. Aad et al. (ATLAS Collaboration), Phys.Lett. **B716**, 1 (2012), 1207.7214.
 - [2] S. Chatrchyan et al. (CMS Collaboration), Phys.Lett. **B716**, 30 (2012), 1207.7235.
 - [3] S. Weinberg, Phys.Rev. **D13**, 974 (1976).
 - [4] M. Papucci, J. T. Ruderman, and A. Weiler, JHEP **1209**, 035 (2012), 1110.6926.
 - [5] G. Aad et al. (ATLAS Collaboration), JHEP **1409**, 015 (2014), 1406.1122.
 - [6] G. Aad et al. (ATLAS Collaboration), Tech. Rep. CERN-PH-EP-2014-143, CERN, Geneva (2014), 1407.0583.
 - [7] G. Aad et al. (ATLAS Collaboration), JHEP **1406**, 124 (2014), 1403.4853.
 - [8] C. Collaboration (CMS Collaboration), Tech. Rep. CMS-PAS-SUS-13-015, CERN, Geneva (2013).
 - [9] C. Collaboration (CMS Collaboration), Tech. Rep. CMS-PAS-SUS-14-011, CERN, Geneva (2014).
 - [10] S. Chatrchyan et al. (CMS Collaboration), Eur.Phys.J. **C73**, 2677 (2013), 1308.1586.
 - [11] G. Aad et al. (ATLAS), Phys.Rev. **D90**, 052008 (2014), 1407.0608.
 - [12] C. Collaboration (CMS Collaboration), Tech. Rep. CMS-PAS-SUS-13-009, CERN, Geneva (2014).
 - [13] G. Aad et al. (ATLAS Collaboration), Eur.Phys.J. **C74**, 2883 (2014), 1403.5222.
 - [14] V. Khachatryan et al. (CMS Collaboration), Phys.Lett. **B736**, 371 (2014), 1405.3886.

- [15] C. Collaboration (CMS Collaboration), Tech. Rep. CMS-PAS-SUS-13-021, CERN, Geneva (2013).
- [16] S. Chatrchyan et al. (CMS Collaboration), Phys.Rev.Lett. **112**, 161802 (2014), 1312.3310.
- [17] G. Aad et al. (ATLAS), JHEP **1310**, 189 (2013), 1308.2631.
- [18] C. Collaboration (CMS Collaboration), Tech. Rep. CMS-PAS-SUS-13-018, CERN, Geneva (2014).
- [19] G. Aad et al. (ATLAS), JHEP **1410**, 24 (2014), 1407.0600.
- [20] C. Collaboration (CMS Collaboration), Tech. Rep. CMS-PAS-SUS-13-008, CERN, Geneva (2013).
- [21] G. Aad et al. (ATLAS), JHEP **1406**, 035 (2014), 1404.2500.
- [22] S. Chatrchyan et al. (CMS), JHEP **1401**, 163 (2014), 1311.6736.
- [23] S. Chatrchyan et al. (CMS), Phys.Rev. **D90**, 032006 (2014), 1404.5801.
- [24] R. Grober, M. Muhlleitner, E. Popena, and A. Wlotzka (2014), 1408.4662.
- [25] P. Agrawal and C. Frugiuele, JHEP **1401**, 115 (2014), 1304.3068.
- [26] M. Muhlleitner and E. Popena, JHEP **1104**, 095 (2011), 1102.5712.
- [27] J. Aebischer, A. Crivellin, and C. Greub (2014), 1410.8459.
- [28] C. Boehm, A. Djouadi, and Y. Mambrini, Phys.Rev. **D61**, 095006 (2000), hep-ph/9907428.
- [29] A. Delgado, G. F. Giudice, G. Isidori, M. Pierini, and A. Strumia, Eur.Phys.J. **C73**, 2370 (2013), 1212.6847.
- [30] K. Rolbiecki and K. Sakurai, JHEP **1309**, 004 (2013), 1303.5696.
- [31] D. Curtin, P. Meade, and P.-J. Tien (2014), 1406.0848.
- [32] J. S. Kim, K. Rolbiecki, K. Sakurai, and J. Tattersall (2014), 1406.0858.
- [33] M. Czakon, A. Mitov, M. Papucci, J. T. Ruderman, and A. Weiler (2014), 1407.1043.
- [34] D. Berenstein, T. Liu, and E. Perkins, Phys.Rev. **D87**, 115004 (2013), 1211.4288.
- [35] E. Alvarez and Y. Bai, JHEP **1208**, 003 (2012), 1204.5182.
- [36] M. S. Carena, J. Espinosa, M. Quiros, and C. Wagner, Phys.Lett. **B355**, 209 (1995), hep-ph/9504316.
- [37] N. D. Christensen, T. Han, and S. Su, Phys.Rev. **D85**, 115018 (2012), 1203.3207.
- [38] M. Carena, S. Gori, N. R. Shah, and C. E. Wagner, JHEP **1203**, 014 (2012), 1112.3336.
- [39] A. Belyaev, S. Khalil, S. Moretti, and M. C. Thomas, JHEP **1405**, 076 (2014), 1312.1935.
- [40] A. Djouadi, M. Muhlleitner, and M. Spira, Acta Phys.Polon. **B38**, 635 (2007), hep-

- ph/0609292.
- [41] W. Beenakker, S. Brensing, M. Kramer, A. Kulesza, E. Laenen, et al., JHEP **1008**, 098 (2010), 1006.4771.
 - [42] A. Broggio, A. Ferroglia, M. Neubert, L. Vernazza, and L. L. Yang, JHEP **1307**, 042 (2013), 1304.2411.
 - [43] C. Borschensky, M. Krmer, A. Kulesza, M. Mangano, S. Padhi, et al., Eur.Phys.J. **C74**, 3174 (2014), 1407.5066.
 - [44] T. Han, S. Padhi, and S. Su, Phys.Rev. **D88**, 115010 (2013), 1309.5966.
 - [45] D. Ghosh, Phys.Rev. **D88**, 115013 (2013), 1308.0320.
 - [46] G. Aad et al., Tech. Rep. ATL-PHYS-PUB-2013-011, CERN, Geneva (2013).
 - [47] G. Aad et al., Tech. Rep. ATL-PHYS-PUB-2014-010, CERN, Geneva (2014).
 - [48] C. Collaboration (CMS Collaboration), Tech. Rep. CMS-PAS-SUS-14-012, CERN, Geneva (2015).
 - [49] J. Alwall, R. Frederix, S. Frixione, V. Hirschi, F. Maltoni, et al., JHEP **1407**, 079 (2014), 1405.0301.
 - [50] T. Sjostrand, S. Mrenna, and P. Z. Skands, JHEP **0605**, 026 (2006), hep-ph/0603175.
 - [51] J. de Favereau et al. (DELPHES 3), JHEP **1402**, 057 (2014), 1307.6346.
 - [52] J. Anderson, A. Avetisyan, R. Brock, S. Chekanov, T. Cohen, et al. (2013), 1309.1057.
 - [53] M. Cacciari, S. Frixione, M. L. Mangano, P. Nason, and G. Ridolfi, JHEP **0809**, 127 (2008), 0804.2800.
 - [54] A. Bredenstein, A. Denner, S. Dittmaier, and S. Pozzorini, Phys.Rev.Lett. **103**, 012002 (2009), 0905.0110.
 - [55] W. Beenakker, S. Dittmaier, M. Kramer, B. Plumper, M. Spira, et al., Nucl.Phys. **B653**, 151 (2003), hep-ph/0211352.
 - [56] J. M. Campbell and R. K. Ellis, JHEP **1207**, 052 (2012), 1204.5678.
 - [57] A. Lazopoulos, T. McElmurry, K. Melnikov, and F. Petriello, Phys.Lett. **B666**, 62 (2008), 0804.2220.
 - [58] T. Han, S. Su, Y. Wu, B. Zhang, and H. Zhang (2015), to appear.